applied sciences

MDPI

Article

Examination of a Human Heart Fabricating Its 3D-Printed Cardiovascular Model and Employing Computational Technologies

Paschalis Charalampous [1,*], Nikolaos Kladovasilakis [1,2], Maria Zoumaki [1], Ioannis Kostavelis [1,3], Konstantinos Votis [1], Konstantinos Petsios [4], Dimitrios Tzetzis [2] and Dimitrios Tzovaras [1]

[1] Centre for Research and Technology Hellas, Information Technologies Institute (CERTH/ITI), 57001 Thessaloniki, Greece; nikoklad@iti.gr (N.K.); mariazita687@gmail.com (M.Z.); gkostave@iti.gr (I.K.); kvotis@iti.gr (K.V.); dimitrios.tzovaras@iti.gr (D.T.)
[2] Digital Manufacturing and Materials Characterization Laboratory, School of Science and Technology, International Hellenic University, 57001 Thessaloniki, Greece; d.tzetzis@ihu.edu.gr
[3] Department of Supply Chain Management, School of Economics and Business Administration, International Hellenic University, 60100 Katerini, Greece
[4] Clinical Research Unit, Onassis Cardiac Surgery Center, 17674 Athens, Greece; petsiosk@gmail.com
* Correspondence: pcharalampous@iti.gr

Abstract: In this paper, an innovative approach concerning the investigation of the human heart is introduced, employing state-of-the-art technologies. In particular, sophisticated algorithms were developed to automatically reconstruct a 3D model of a human heart based on DICOM data and to segment the main parts that constitute it. Regarding the reconstructed 3D model, a diagnosis of the examined patient can be derived, whereas in the present study, a clinical case involving the coarctation of the aorta was inspected. Moreover, numerical approaches that are able to simulate flows on complex shapes were considered. Thereupon, the outcomes of the computation analysis coupled with the segmented patient-specific 3D model were inserted in a virtual reality environment, where the clinicians can visualize the blood flow at the vessel walls and train on real-life medical scenarios, enhancing their procedural understanding prior to the actual operation. The physical model was 3D-printed via the MultiJet 3D printing process utilizing materials possessing an adequate mechanical response replicating the mechanical properties and the geometrical characteristics of the human heart. The presented tools aim at the creation of an innovative digital environment, where gaining surgical experience and developing pre-operative strategies could be achieved without the risk and anxiety of actual surgery.

Keywords: cardiology; additive manufacturing; computational fluid dynamics; virtual reality; 3D reconstruction

check for updates

Citation: Charalampous, P.; Kladovasilakis, N.; Zoumaki, M.; Kostavelis, I.; Votis, K.; Petsios, K.; Tzetzis, D.; Tzovaras, D. Examination of a Human Heart Fabricating Its 3D-Printed Cardiovascular Model and Employing Computational Technologies. *Appl. Sci.* **2023**, *13*, 10362. https://doi.org/10.3390/app131810362

Academic Editor: Qiang Cheng

Received: 25 August 2023
Revised: 12 September 2023
Accepted: 14 September 2023
Published: 16 September 2023

Copyright: © 2023 by the authors. Licensee MDPI, Basel, Switzerland. This article is an open access article distributed under the terms and conditions of the Creative Commons Attribution (CC BY) license (https://creativecommons.org/licenses/by/4.0/).

1. Introduction

The inspection of a human heart on a regular basis is critical aiding in the diagnosis and treatment of a wide range of heart-related conditions, such as coronary artery disease, arrhythmias, heart valve disease, and congenital heart defects. In addition, along with the examination of the heart's structure, function, and blood flow, healthcare professionals can potentially identify abnormalities and malfunctions of the heart, as well as develop appropriate treatment plans. Furthermore, the examination of the heart is necessary for monitoring the progress of heart-related conditions and for evaluating the effectiveness of the treatment. Concerning medical and clinical research, the investigation of a human heart using cutting edge technologies is essential for understanding how the heart operates and for developing new treatments, therapies, and surgical strategies for heart-related conditions. More specifically, in recent years, researchers and clinicians have utilized advanced imaging techniques to study the heart's anatomy and function [1] and computational simulations to study the hemodynamics of blood flow through the heart [2]. Moreover, artificial intelligence (AI) algorithms are applied to analyze large amounts of patient data, making more accurate predictions of disease progression, treatment outcomes, and complications [3]. Finally, additive manufacturing (AM) procedures are employed to construct identical models of human hearts [4].

VR technology can be employed in cardiology to simulate the human heart in an interactive and immersive manner. Hereupon, healthcare professionals and medical students can experience a detailed and realistic representation of the heart, allowing for an enhanced understanding of its structure and function [5]. The main idea is to use medical imaging data, such as magnetic resonance imaging (MRI) or computed tomography (CT) scans, to create 3D models of the heart that can be imported into a virtual environment. Once inside the virtual environment, the users can interact with the heart model in various ways, such as zooming in on specific areas, rotating the heart to view it from different angles, as well as highlighting different structures of interest. The VR software can also provide additional information about the heart, such as its blood flow, the different parts of the heart, and how it functions [6]. Furthermore, VR technology can also be applied in medical training to simulate demanding surgeries in such a way that medical students and healthcare professionals could practice in a safe and controlled environment improving that way their skills reducing the risk of errors during real-life procedures.

Computational fluid dynamics (CFD) composes a powerful analysis tool that can be used to evaluate the flow of blood in the human heart with the aid of numerical simulations, providing valuable insights into the hemodynamics of the heart, such as blood pressure, flow rates, and velocity profiles. In particular, CFD simulations can be applied to study the progression and development of cardiovascular diseases, such as aneurysms and atherosclerosis [7]. Through analyzing the flow patterns in the heart, researchers can identify areas of high shear stress and turbulence, which can lead to the formation of plaque and other disease-related conditions. Another sector in which these numerical analyses are utilized is in the design and optimization of medical devices, such as heart valves and stents, where the developed CFD models are capable of identifying potential blockages or turbulences in the heart. Moreover, CFD simulations are considered prior to cardiovascular operations in order to enhance the surgical strategy in coronary artery bypass surgery and heart transplant cases [8].

One of the most promising technologies that have been employed in recent years in the inspection of cardiovascular diseases is the AM process, which is used to create a highly detailed and accurate physical replica of a human heart [9,10]. AM procedures utilize a layer-by-layer approach to construct objects from digital designs; hence, a 3D model of the heart can be fabricated in order to accurately represent its shape, size, and structure. It must be noted that certain AM technologies can provide the ability to construct 3D models with tissue-like materials [11,12]. These physical 3D-printed models could be a valuable educational tool for medical students and healthcare professionals, allowing them to examine the heart in greater detail and gain a better understanding of its anatomy and function [13]. However, certain challenges such as the quality of the medical imaging data derived from MRI or CT scanning procedures, as well as the duration and the expertise that is necessary for the 3D modeling of patient-specific hearts, need to be addressed.

The objective of the present study is the development of novel technological tools based on cutting-edge applied sciences such as 3D modeling, VR, numerical simulation, and the additive manufacturing of complex cardiac models. In particular, the novelty of the present research can be summarized in the next remarks:

- The 3D modeling of patient–specific human hearts using a robust and fast 3D reconstruction and segmentation tool that does not require the purchase of dedicated software packages or special training on its operation;
- The development of a sophisticated virtual reality environment that provides the necessary technological assets in order to inspect a human heart, providing a unique

and valuable learning experience for healthcare professionals, medical students, and patients;
- The visualization of complex simulations for professional clinicians, which can be a valuable tool in studying the hemodynamics of the human heart, designing medical devices, or even planning surgical procedures in the developed VR environment;
- The fabrication of additively manufactured human hearts utilizing heart-like materials in order to produce a detailed replica of the real one, highlighting potential heart defects or allowing scientists and doctors to study the structure as well as the function of the heart in greater detail.

2. Materials and Methods

In the first step of the proposed methodology, the automatic reconstruction of the heart's 3D model is conducted considering medical data that are based on the Digital Imaging and Communications in Medicine (DICOM) protocol [14]. These data are obtained directly from CT scans and contain 2D information about the examined clinical case. In addition, clustering algorithms like spectral graphs [15] and k-means [16] are utilized to segment the major parts of a human heart. With the aid of the reconstructed and segmented patient-specific 3D model of the heart, clinicians can diagnose potential defects. The next section is associated with the applied methodologies of developing numerical approaches investigating the hemodynamics of the examined CoA case, applying CFD models as well as presenting the VR environment where several tools can aid the clinician in establishing optimal pre-operative strategies. Furthermore, a patient-specific physical model was 3D-printed, applying an opaque resin that possesses mechanical properties similar to the actual cardiac muscle tissue [11]. The results of the introduced study highlight the uniform blood flow distribution and velocity profile in the narrowed region of the heart. Moreover, various tools, such as manipulating the 3D model of the heart, making sections, measuring distances, as well as integrating medical devices like mechanical valves in the VR environment are also documented. In addition, the dimensional accuracy of the AM process was evaluated via the employment of a 3D structural laser scanner that scanned the 3D-printed aorta and correlated it with the corresponding 3D digital model. Finally, the main conclusions of the study and some prospects for future research are outlined. The applied workflow concerning the present research paper is illustrated in Figure 1.

2.1. Data Pre-Processing

The first step of the employed methodology is to analyze the input data stored in the DICOM format, which were collected from CT scans and utilized to model the investigated human heart. The DICOM protocol represents medical data in a specific format that are concentrated mainly in medical imaging and also contains certain metadata that are useful to compute the Hounsfield Unit (HU). The HU constitutes a relative quantitative metric of radiodensity that is implemented by radiologists and clinicians in order to enhance their interpretation of the outcome of the CT scan process [17]. In particular, the attenuation–absorption of radiation within tissue during the CT procedure is used to create grayscale images with the aid of certain DICOM metadata, where the conversation of raw pixel data to the Hounsfield scale is feasible. In general, dense tissue absorbs significant X-rays representing brighter areas, whereas less-dense tissues lead to dark regions in the image. Considering the abovementioned information, a particular set of data could be extracted, such as bones, in situations where the proper threshold is selected.

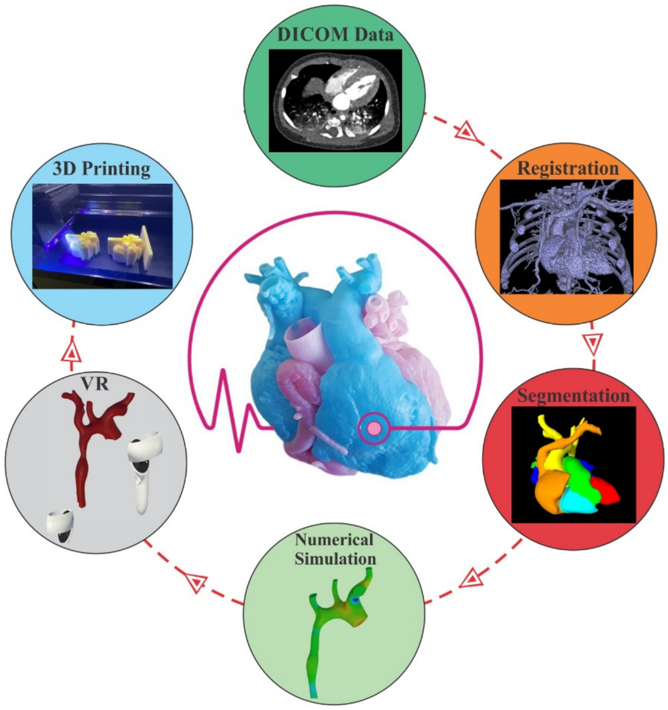

Figure 1. Workflow of the research study.

2.1.1. CT Scan Reconstruction

The marching cubes algorithm was applied in the present research study; it consists in a computational method utilized to create 3D surface representations of complex data, such as medical images [18,19]. In the first phase of the algorithm, the space that is specified by the DICOM data is converted into a grid of voxels, which consists of 3D pixels representing the values of grayscale at each location. It must be noted that the proper selection of the intensity range of HU is essential since diverse tissues and structures in the human body possess different densities and therefore different ranges of HU. The core objective of the methodology is the determination of a potential surface that belongs to the 3D model (bone, organ, etc.) in each of these investigated voxels, taking into account an intensity range of values that are related to the gray tone of the examined voxel's vertices. This stage could be illustrated via a marching of a theoretical cube into a scalar field, in which the absence or presence of a boundary surface in each vertex of the cube is categorized in one of the potential generated surface polygons [18]. This process is terminated after the investigation of the whole examined scalar field (all the voxels of the scene); hence, a 3D model is constructed with a polygonal approximation of the generated surfaces through connecting the vertices of all the traversed cubes. The employed methodology is schematically illustrated in Figure 2a, where the main functions of the automatic 3D reconstruction module considering DICOM data as input are displayed.

In the next phase, filtering methods are utilized in the generated 3D mesh, enabling the removal of parts that do not belong to the investigated heart model. In the present case, several bones that are not directly attached to the heart, like the scapula, clavicle, sternum, as well as spine bones, were removed from the scene using the open3d library [20]. In particular, a function that clusters connected triangles was applied, i.e., triangles that are connected via edges are assigned the same cluster index in order to remove small parts that are produced and should be removed from the scene. Moreover, a reference 3D model of a heart was aligned with the examined one using the Iterative Closest Point (ICP) algorithm, which can be applied in order to minimize the differences between two point clouds [21]. Hereupon, parts of the reconstructed model that possessed a certain distance to the reference were removed from the 3D model of the heart. In addition, algorithms concerning the removal of outliers and noise were also applied in order to isolate the examined heart. Finally, the extracted mesh was further edited with processes like hole-filling, smoothing, etc., in order to secure the correctness and continuity of the meshes. The generation of the 3D mesh as well as the influence of the filtering methods in the captured scene, coupled with the final outcome of the employed methodology, are demonstrated in Figure 2b.

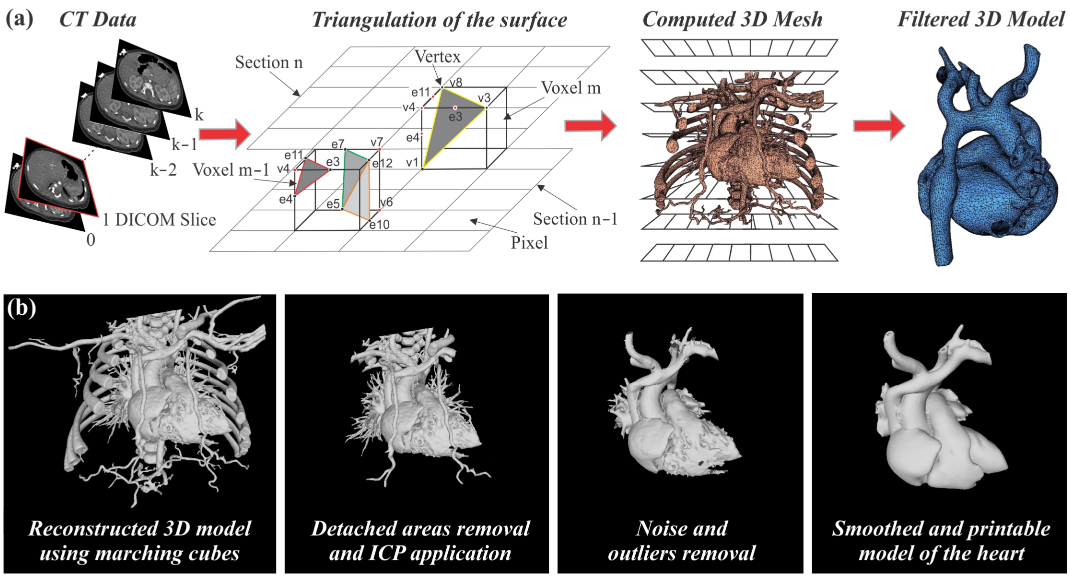

Figure 2. (**a**) Steps for the 3D reconstruction process. (**b**) Outcomes of the applied methodology concerning the investigated clinical case.

2.1.2. Human Heart Segmentation

The next step of the developed methodology is the segmentation of the human heart, which poses a challenging task due to its complex shape and variability [22]. However, the accurate segmentation of the heart is critical for many clinical applications such as planning for cardiac interventions and treatments, the quantification of cardiac function, and the diagnosis of various cardiac diseases. Human heart segmentation refers to the process of identifying and separating the main regions of the heart. In the present study, the spectral clustering algorithm was considered [23] to cluster six main parts of the heart such as the aorta, the right/left atrium, the right/left ventricle, and the pulmonary artery. In the first step of the segmentation process, an adjacency map is constructed, reading all the vertices and the faces of the reconstructed heart 3D model that was determined in the previous paragraph. Hereupon, knowing all the connected edges of the 3D point cloud of the reconstructed heart, a distance matrix is developed that takes into account the geodesic as well as the angular distance between all the adjacent faces of the model. In the next phase, the affinity matrix A is established, determining how similar or close two points are in the 3D space, and is defined as [24]:

$$A[i][j] = exp\frac{-d^2(s_i.s_j)}{\sigma^2} \tag{1}$$

where d (s_i, s_j) is a distance metric mentioned earlier, σ composes a scale parameter selected manually, and S is a set of points $S = \{s_1, s_2, \ldots, s_n\}$ that need to be clustered into k (six in the examined case) subsets. If $A[i][j] = 0$, this means that the vertices s_i and s_j are not connected via an edge. The subsequent step is the definition of the diagonal degree matrix D as in [25] and the construction of the Laplacian L (Equation (2)):

$$D[i][i] = \sum_{J=1}^{n} A[i][j] \tag{2}$$

$$L = D^{-1/2} A D^{-1/2} \quad (3)$$

The methodology of the spectral clustering algorithm suggests the computation of the first k eigenvectors $u_1, u_2, \ldots, u_k$ of the Laplacian L as well as the creation of the matrix $U = [u_1, u_2, \ldots, u_k]$, redefining the input space as a k-dimensional space [25]. It must be noted that the eigenvectors are ordered according to their corresponding eigenvalues. Finally, the clustering of this subspace can be accomplished via the utilization of a standard clustering technique like the k-means algorithm, producing k clusters for the investigated human heart.

Results of the employed methodology are displayed in Figure 3, wherein the left part a subsampled model of the reconstructed model of the heart is displayed. Due to computational time, the spectral clustering algorithm is first executed on a subsampled 3D model. Nevertheless, the segmentation of the full-heart reconstructed 3D model was also conducted via the iteration of each vertex and its calculation to the closest vertex of the subsampled model, thus reducing the computational time. Finally, depending on the cluster of the closest vertex, the corresponding vertex of the dense 3D model was assigned to a similar cluster. Even though the vertices that are located close to the borders of the clusters can potentially be placed in the wrong part of the heart, the gain in the computation time compensated the restricted number of misplaced vertices. It should be noted that manual post-processing of the segmented 3D model could lead to an ideal representation of the examined heart, repairing potential imperfections of the reconstructed heart, as shown in the next paragraphs.

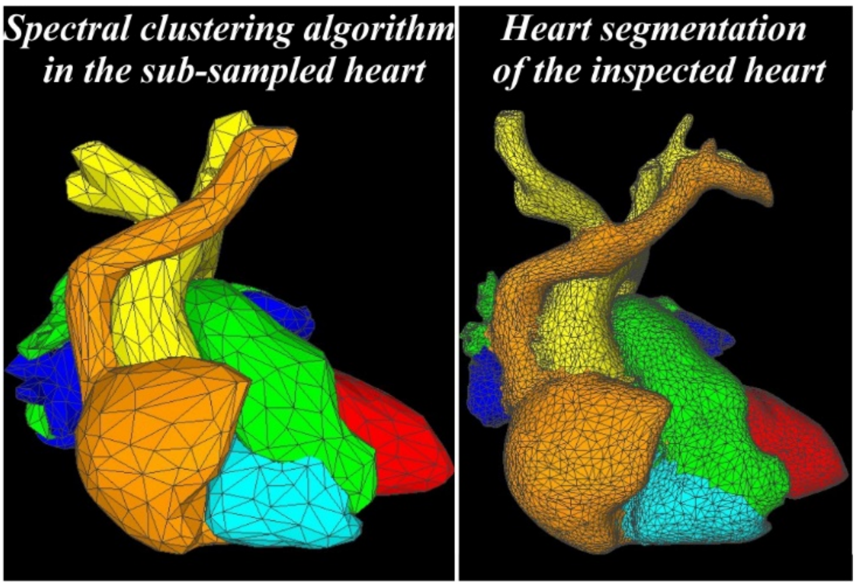

Figure 3. Clustering results of the employed methodology in the examined heart.

In the left part of Figure 4, the examined segmented aorta is illustrated as it was derived from the clustering process, exhibiting a typical case of coarctation of the aorta (CoA). CoA is a relatively common birth defect that accounts for 6–8% of all congenital heart defects, presenting a narrower aorta than the usual [26]. In situations where the narrowing is very severe, that could lead to congestive heart failure or insufficient blood flow to the organs of the body [27]. Hereupon, the diagnosis of such defects should be accurate in a timely manner in order for the patient to possess the expected opportunity for a positive health outcome, taking into account that clinical decision-making will be tailored to a correct awareness of the patient-specific health issue [28]. It should be noted that the extracted model of the aorta was post-processed using the open-source software Meshmixer v3.5 in order to repair and finish the reconstructed model via its inspection tools like hole detection, disconnected components, and non-manifold areas. The outcome of this process is demonstrated in the right part of Figure 4 exhibiting the 3D model of the Aorta that was considered in the upcoming numerical investigations.

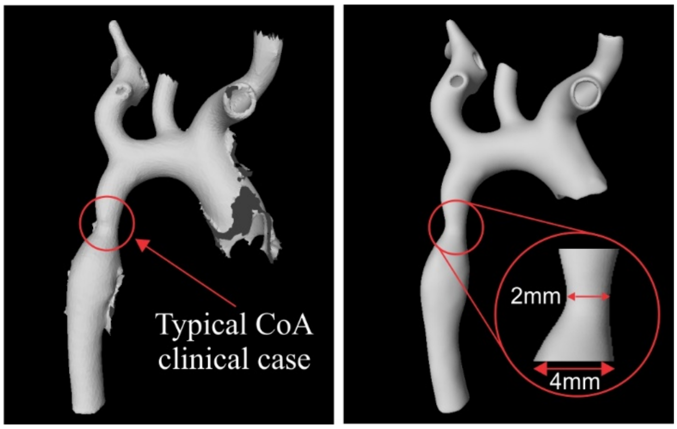

Figure 4. The segmented 3D model of the aorta, exhibiting its coarctation.

2.2. Applied Methodology

2.2.1. Numerical Model

Along with the observation of the CoA on the reconstructed 3D model, a numerical evaluation of the influence of this defect in the bloodstream was investigated. For this reason, CFD analyses were performed, utilizing the ANSYS™ Fluent module, in order to extract the pressure and velocity contours that quantify the blood flow in the cardiovascular system of the examined patient. In the context of this study, two different CFD analyses were conducted; the first one takes into account the reconstructed 3D model with the CoA, and in the second case, the examined aorta was modified through eliminating the defect and normalizing the aorta's walls correspondingly with the surfaces before and after the defect. It is worth noting that the internal volumes were used as control volumes for the bloodstream.

Taking into account the existing literature [29], the conditions concerning the bloodstream inside the aorta were selected with the following assumptions. First, the blood was assumed to be an incompressible Newtonian fluid with a constant density (ρ) of 1060 kg/m^3 and a constant viscosity (μ) of 0.004 Pa·s (4 cP) [30,31]. Furthermore, the boundary conditions regarding the arterial walls were set as stationary and rigid, with their elasticity and thickness set to be negligible. Regarding the initial boundary conditions, the inlet of the blood stream was applied on the ascending aorta with an initial velocity of 1.37 m/s, which is the mean blood velocity for an aorta according to published studies [32]. In addition, at the outlets, the initial pressure gauge (vessels and descending aorta) was evaluated at 100 mmHg (13,332 Pa) [33]. The ANSYS solver employed the Navier–Stokes formulation for the conservation of momentum of an incompressible flow in the three dimensions (R^3), as it is listed below [31], where u represents the velocity, p is the pressure, t is the time, and μ is the viscosity.

$$
\begin{aligned}
x: \frac{\partial u_x}{\partial t} + u\nabla u_x &= -\frac{1}{\rho}\frac{\partial p}{\partial x} + \mu\left(\nabla^2 u_x\right) \\
y: \frac{\partial u_y}{\partial t} + u\nabla u_y &= -\frac{1}{\rho}\frac{\partial p}{\partial y} + \mu\left(\nabla^2 u_y\right) \qquad (4) \\
z: \frac{\partial u_z}{\partial t} + u\nabla u_z &= -\frac{1}{\rho}\frac{\partial p}{\partial z} + \mu\left(\nabla^2 u_z\right)
\end{aligned}
$$

Furthermore, the k-ε turbulence model was utilized for the turbulence flow simulation, where k is the turbulence kinetic energy, ε represents the rate of dissipation, μ_t is the turbulence (known as eddy) viscosity, G_k represents the generation of turbulence kinetic energy due to the mean velocity gradients, G_b is the generation of turbulence kinetic energy due to buoyancy, and Y_M represents the contribution of the fluctuating dilatation in compressible turbulence to the overall dissipation rate. Furthermore, the flow coefficients coupled with their values are as follows: C_μ = 0.09, σ_k = 1, σ_ε = 1.3, $C_{1\varepsilon}$ = 1.44, $C_{2\varepsilon}$ = 1.92, and $C_{3\varepsilon}$ = 1 [31]. These values have been determined from experiments for fundamental turbulent shear flows including homogeneous shear flows and decaying isotropic grid turbulence according to ANSYS Fluent documentation [34]. They have been found to work fairly well for a wide range of wall-bound and free shear flows. Below, the k-ε formulations are presented, where i, j = 1, 2, 3 and x_i is the corresponding axis:

$$\text{Turbulence (eddy) viscosity}: \ \mu_t = \rho C_\mu \frac{k^2}{\varepsilon}$$

$$\text{Turbulence energy}: \ \rho\frac{\partial k}{\partial t} + \rho\frac{\partial (k u_i)}{\partial x_i} = \frac{\partial}{\partial x_j}\left[\left(\mu + \frac{\mu_t}{\sigma_k}\right)\frac{\partial k}{\partial x_j}\right] + G_k + G_b - \rho\varepsilon + Y_M \tag{5}$$

$$\text{Energy consumption}: \ \rho\frac{\partial \varepsilon}{\partial t} + \rho\frac{\partial (\varepsilon u_i)}{\partial x_i} = \frac{\partial}{\partial x_j}\left[\left(\mu + \frac{\mu_t}{\sigma_\varepsilon}\right)\frac{\partial \varepsilon}{\partial x_j}\right] + C_{1\varepsilon}\frac{\varepsilon}{k}(G_k + C_{3\varepsilon}G_b) - C_{2\varepsilon}\rho\frac{\varepsilon^2}{k}$$

Due to the unique morphology of the examined aorta, fine meshes of tetrahedral elements were applied in order to achieve mesh-independent results. The minimum element's size was selected at 200 μm and meshes with total elements of approximately 500,000 were utilized for the development of the numerical simulations. The aforementioned flow conditions, formulations, and meshes were utilized along with the COUPLED flow solver of ANSYS and the maximum number of solving iterations at 300. Finally, the value of 0.001 was selected for all residuals as the convergence criterion for the CFD problem, providing accurate and reliable solutions.

2.2.2. VR Environment

The human heart is a complex organ that requires extensive knowledge and skills to properly examine and diagnose any defects. With advancements in technology, VR has emerged as a promising tool for medical professionals, aiding in pre-operational procedures. Therefore, an approach is presented using the Oculus Quest 2 and Unity to develop a VR environment for examining the human heart. In particular, the Oculus Integration asset was imported to the Unity platform in order to enable the user to interact with the VR tool using an Oculus Quest 2. In particular, a section tool of the heart's 3D model was developed based on [35], enriching it with several adaptations in order to allow the user to make sections throughout the heart at specific points. The introduced VR application provides a comprehensive and interactive platform for medical doctors to examine the human heart and diagnose any issues pre-operatively. With continued advancements in VR technology, this tool has the potential to significantly improve pre-operational procedures for the examination of the human heart. In addition, the VR module includes the ability to zoom in at a specific point of interest as well as to navigate internally within the investigated heart for a more detailed examination, providing better supervision of the clinical case and enabling the user to make robust decisions concerning the pre-operational procedure.

Another asset that the developed VR platform can support is recording notes at any point in the heart wherever the doctor/user deems necessary. This tool is particularly useful for annotating any abnormalities or observations generated during the examination of the patient. Moreover, the application includes a measuring feature that allows the user to measure the distance between various points of the heart. This feature can be used to assess the dimensions of several parts of the heart and identify any potential issues [36]. Finally, the VR menu provides a visualization of the CFD results of the heart, aiding in the diagnosis and treatment of various heart-related conditions through providing a more comprehensive understanding of the heart's function. All of the aforementioned technological tools are thoroughly described in the next section.

2.2.3. Additive Manufacturing and 3D Scanning Procedures

The main objective of the applied AM process is the construction of 3D-printed heart models that possess similar properties to the actual heart tissue, hence the material jetting AM technology was employed utilizing the ProJet MJP 5600 3D Systems™ 3D printer. The material jetting (MJ) process uses inkjet printing techniques to selectively deposit droplets (voxels) of photopolymer material through the jets of the printhead and solidify them with the aid of UV lights, resulting in the creation of the desired part [37]. The main advantage of this process is the ability of multi-material 3D printing, i.e., the fabrication of components consisting of two or more composite materials transfusing different properties in different regions. Therefore, in order to imitate the basic properties of heart tissue, such as elasticity and strength, the MJ technique was employed in the present work. According to the manufacturer's datasheet, the composite material with the closest properties to heart tissue [11,38] is RWT-ENT A50™. RWT-ENT A50™ is a composite material consisting mainly of VisiJet CE-NT™ (elastomer material) and small portions of VisiJet CR-CL 200™ (rigid material). Table 1 lists the main properties of heart tissue measured in a passive state and the employed materials for the 3D printing process. Finally, the maximum resolution of 750 × 750 × 2000 DPI and the minimum layer height of 13 µm were applied, leading to a sufficiently fast 3D printing process of around 29 h per heart model and 12 h per aorta, achieving the maximum dimensional accuracy of the employed 3D printer.

Table 1. Main elastic properties of the employed materials.

Material	Density [g/cm^3]	Elastic Modulus [MPa]	Tensile Strength [MPa]	Elongation at Break [%]
Heart tissue	1.055	2.84	0.19	-
RWT-ENT A50	1.128	3.56	0.53	65
VisiJet CE-NT™	1.120	0.35	0.3	195
VisiJet CR-CL 200™	1.160	1750	36.5	18

In the context of this study, the 3D models of the heart and aorta were evaluated in terms of dimensional accuracy, utilizing the HP PRO S3 3D Structured Light Scanner (SLS). The HP PRO S3 3D SLS is a desktop 3D scanner that uses the structured light technique to capture the desired 3D geometry, and it is suitable for the scanning of relatively small objects (30–500 mm). Furthermore, this scanner is able to capture high-definition data, up to 2,300,000 vertices per scan, performing with a scan accuracy of 0.1% of the scan size. In detail, three different 360° scans were conducted with three different object orientations to ensure the total scanning of the objects. The dimensional accuracy inspection was performed with CloudCompare software, comparing the digital 3D models that were reconstructed from CT scans with the scanned 3D-printed hearts. Finally, the evaluation process was conducted via the employment of the surface distance map (SDM) methodology as well as the calculation of the mean absolute error (MAE) and root mean square error (RMSE) parameters.

3. Results and Discussion

3.1. CFD Analysis

The conducted CFD analyses sufficiently simulated the flow field inside the examined aorta arteries, evaluating their main physical quantities, such as flow's pressure distribution and flow's velocity magnitude, as it is depicted in Figure 5. Furthermore, via CFD analyses, the main indicators that show abnormalities in the flow, such as pressure losses, energy losses, and mass flow, were accurately calculated, quantifying the size of the cardiovascular problem. It is worth mentioning that an aorta without the defect was used as a benchmark of how blood flow should have been in case the CoA defect was eliminated.

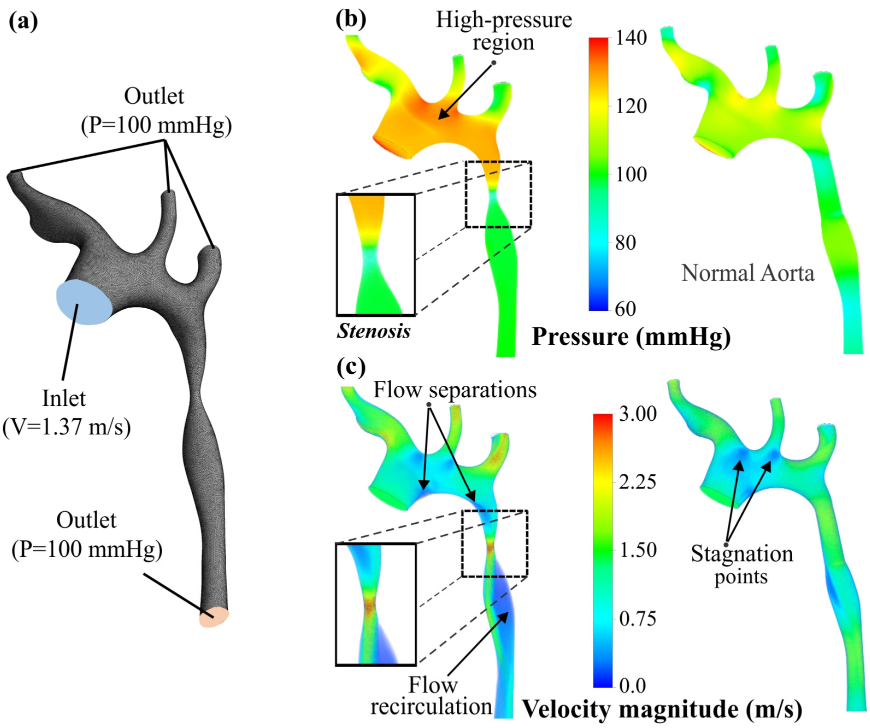

Figure 5. (**a**) Applied CFD model, (**b**) pressure distribution, and (**c**) velocity magnitude for the aorta with CoA coupled with superimposed images of the stenosis (**left**) and for the aorta without CoA (**right**).

More specifically, Figure 5a portrays the employed CFD model and Figure 5b portrays the pressure distribution for the aorta with a CoA defect on the left side and the normal one on the right side. The pressure inside the examined aorta's model ranges between 60 mmHg to 140 mmHg, with the nominal mean pressure for the non-defected aorta set at 100 mmHg, leading to an intense fluctuation concerning the developed pressure values. In addition, in the CoA case, a high-pressure region occurred in the ascending aorta with pressure values from 120 mmHg to 140 mmHg due to the severe stenosis of the artery at the beginning of the descending aorta. As expected, a rapid drop in the pressure (around 70 mmHg) in the stenosis region resulted in discontinuities in the blood flow. On the other hand, the aorta without any defect revealed a more uniform pressure distribution within the flow field, with values ranging between 80 mmHg to 130 mmHg. It is noteworthy that only a few individual peaks of pressure (130 mmHg) occurred at specific stagnation points of the blood flow due to the aorta's morphology. Figure 5c shows the developed velocity magnitudes for the investigated aortas. The aorta with the stenosis revealed extensive and rapid changes in blood flow velocity ranging from 0 m/s to 3 m/s. In addition, the increased pressure in the ascending aorta caused an increase in the velocity of the outlet vessels, and the rapid changes in the flow pressure led to flow separation right before the stenosis, thus disrupting the flow and triggering turbulence phenomena. Moreover, in the stenosis region, a maximum velocity of almost 3 m/s was observed with a 'high velocity' flow jet (around 1.5 m/s) after the stenosis in the left side of the artery, resulting in significant flow recirculation and an increase in the turbulence flow. In contrast, the aorta without the defect presented a uniform velocity magnitude, with values ranging between 0.35 m/s to 2.1 m/s. The observed flow in the descending aorta was mainly laminar, with only minor flow separations due to the non-uniform geometry of the artery.

Taking into account the aforementioned analysis, it is obvious that the investigated CoA case caused a significant disruption of the blood flow inside the aorta, with intense flow separations, flow recirculation, and turbulence insertion. These phenomena resulted in severe pressure and energy losses in the flow and a significant reduction in the mass flow through the descending aorta, as it is documented in Table 2. In detail, the pressure and energy losses tripled in the aorta with the CoA compared to the non-defective aorta, mainly due to flow recirculation and the increased turbulence intensity that the stenosis caused. Furthermore, in the outlet of the descending aorta (after the stenosis), a severe mass flow reduction was observed, with almost 30% of the mass flow for a non-defective aorta. This occurred due to the existence of stenosis and the increase in the mass flows (flow velocity) in the other outlet vessels. To conclude, the stenosis on the examined aorta is critical, causing flow disruptions that could result in long-term hypertension, increased risk of dysfunction of the left ventricle, or even blood shortage to the lower part of the body [39].

Table 2. Quantitative values of the influence of the examined defect.

Model	Pressure Losses (Δp)	Energy Losses	Mass Flow through the Descending Aorta
Aorta with CoA	3906 Pa	3.685 J/kg	6.31 g/s
Aorta without CoA	1296 Pa	1.222 J/kg	21.1 g/s

3.2. VR Environment

The present section describes the implementation of a VR platform in order to visualize and inspect clinical cases of patient-specific hearts' 3D models. A digital library contains the reconstructed and segmented heart models of all the examined cases, categorizing them in relation to the type of their defect. In general, the VR application provides an immersive and interactive approach for users to meticulously explore patient-specific 3D models or study several heart diseases. The developed application allows the user to interact with the 3D model of a heart in a virtual environment using an Oculus VR headset and controllers as illustrated in Figure 6. More specifically, the user can manipulate the heart's scale, select and edit specific parts of the heart, navigate through the heart, make sections at any point, and even record notes at any location within the heart. To achieve these features, the VR module utilizes the Oculus Integration asset tool, which allows the user to grab, transform, and interact with the investigated 3D model. The heart model is divided into specific parts or child objects, each one with a simplified triggered mesh collider that enables them to interact with the controls. The Oculus Integration Library offers a wide range of applications that can be employed for the heart object, allowing the user to hold, move, and scale the heart via the controllers. In addition, the application includes a feature to visualize each segmented part separately, considering the clustering algorithm presented in a previous paragraph.

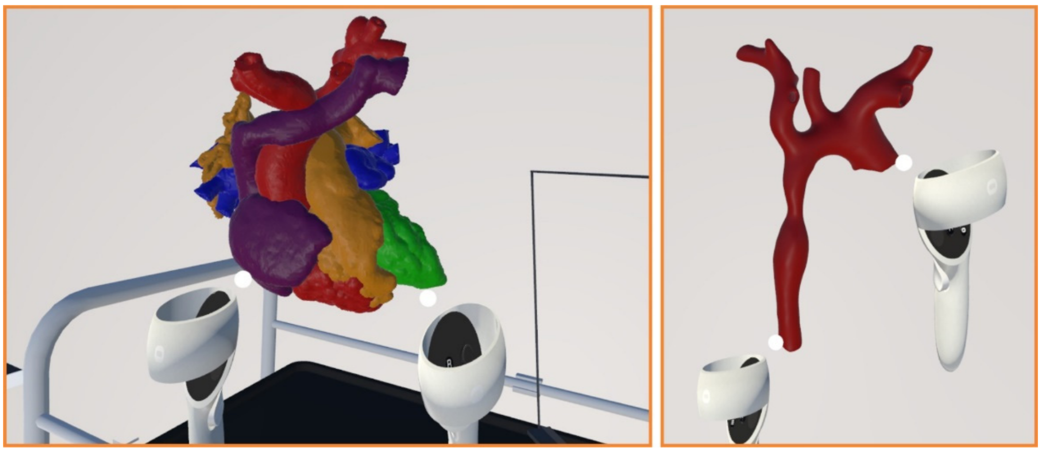

Figure 6. The developed VR environment inspecting a segmented human heart and an aorta.

A typical application of the cross-section tool is depicted in Figure 7, where a parallelepiped space is defined, thus creating a plane where the cross-section or 'cutting' effect occurs. The 'parent' object for these quads is an intractable entity composed of a cylindrical handle and a 3D rectangular frame. The outcome of the module is not only aesthetically pleasing but also user-friendly. Furthermore, the VR application features an annotation tool for attaching notes either on the surface or within the interior of the heart, providing a virtual keyboard and complemented by speech-to-text capabilities. Another valuable feature for medical professionals is a measurement tool that can be used by clinicians to measure any anatomical feature of interest with great precision, such as the diameter of the aorta. Hereupon, the quick determination of abnormalities, such as aneurysms or stenosis, becomes simpler and more efficient. The ability to measure distances between various points within the heart can also support the planning of surgical procedures, allowing physicians to gain a better understanding of the heart's size and defects. It must be noted that all the above-mentioned software tools of the VR application are provided in an intuitive and user-friendly interface, making it easy for medical professionals to use without extensive training or expertise in VR technology, as shown in the next figure.

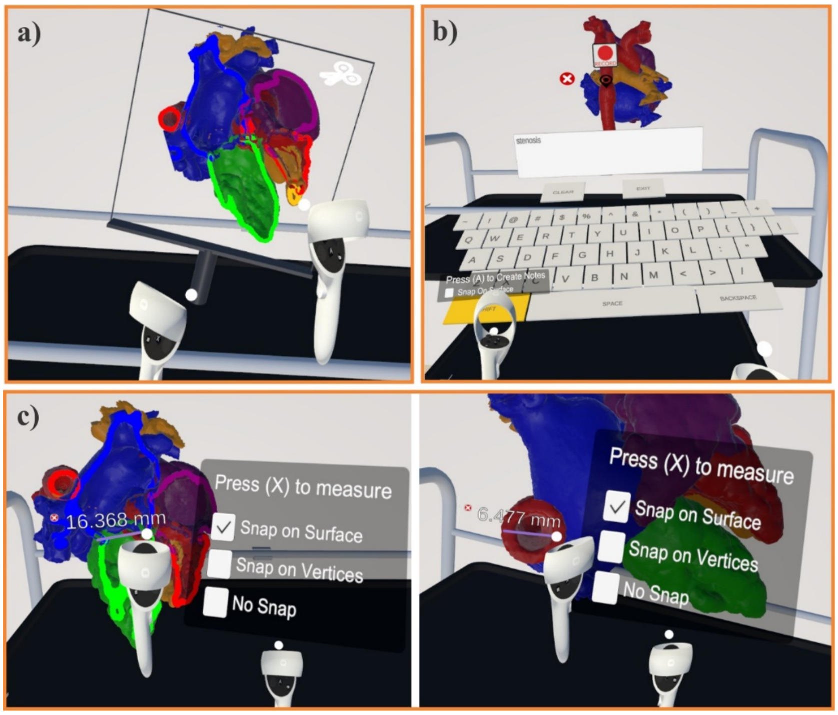

Figure 7. (**a**) Section tool, (**b**) annotation, and (**c**) measurement feature in the VR environment.

Another promising feature that the introduced VR tool provides is the investigation of the numerical analysis within the virtual environment, as presented in Figure 8. The outcomes of the CFD analysis can be imported into the application, allowing a medical doctor who is unfamiliar with these technologies to visualize the blood flow distribution and velocity, thus aiding in the diagnosis and treatment of the patient. In addition, the VR environment provides users the ability to place the appropriate artificial valve on the examined heart, which can be accomplished via the selection of a typical valve from a digital library and evaluating its placement. The integration of such functional tools in a friendly and easy-to-use VR environment grants health professionals the ability to optimize their surgical strategy, thus providing enhanced care to their patients. Overall, the developed technological modules compose a crucial aspect of the VR application, which can greatly enhance the accuracy and efficiency of medical diagnoses and treatment planning.

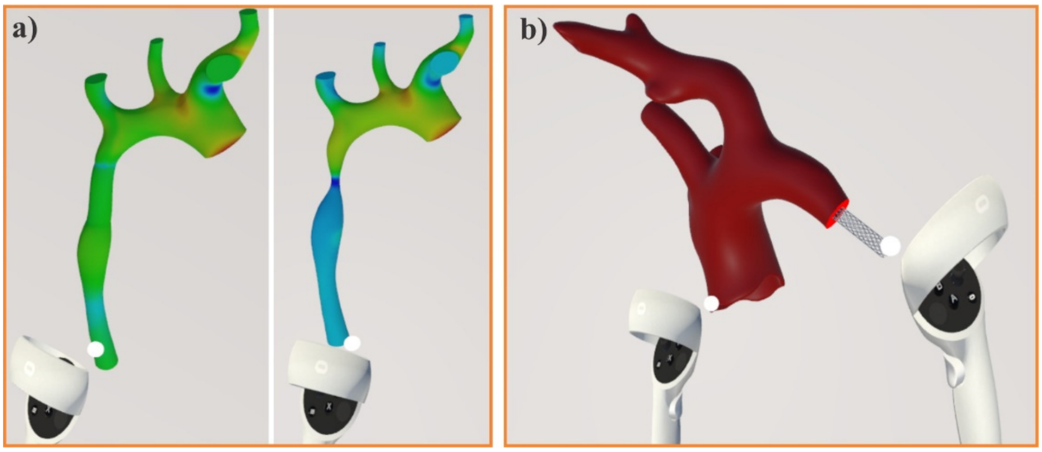

Figure 8. (**a**) Visualization of the results of CFD simulation and (**b**) placement of an artificial valve using the developed VR platform.

3.3. Evaluation of the AM Procedure

Taking into account the automatic 3D reconstruction and segmentation methodology, a patient-specific digital 3D model is extracted for the entire heart and its aorta artery, as illustrated in Figure 9. In detail, Figure 9a shows the final digital 3D model of the heart (left side) and aorta (right side), consisting of approximately 1,090,000 and 371,000 facets, respectively. Furthermore, Figure 9b portrays the 3D-printed models for the heart and the aorta constructed with the RWT-ENT A50 composite material employing the MJP 5600 3D printer. The external dimensions of the examined heart and aorta were 60.91 × 80.36 × 65.79 mm and 39.54 × 45.82 × 74.19 mm, respectively. Finally, it is worth noting that the 3D-printed models were structurally flawless, without any visible defect experiencing extensive elasticity.

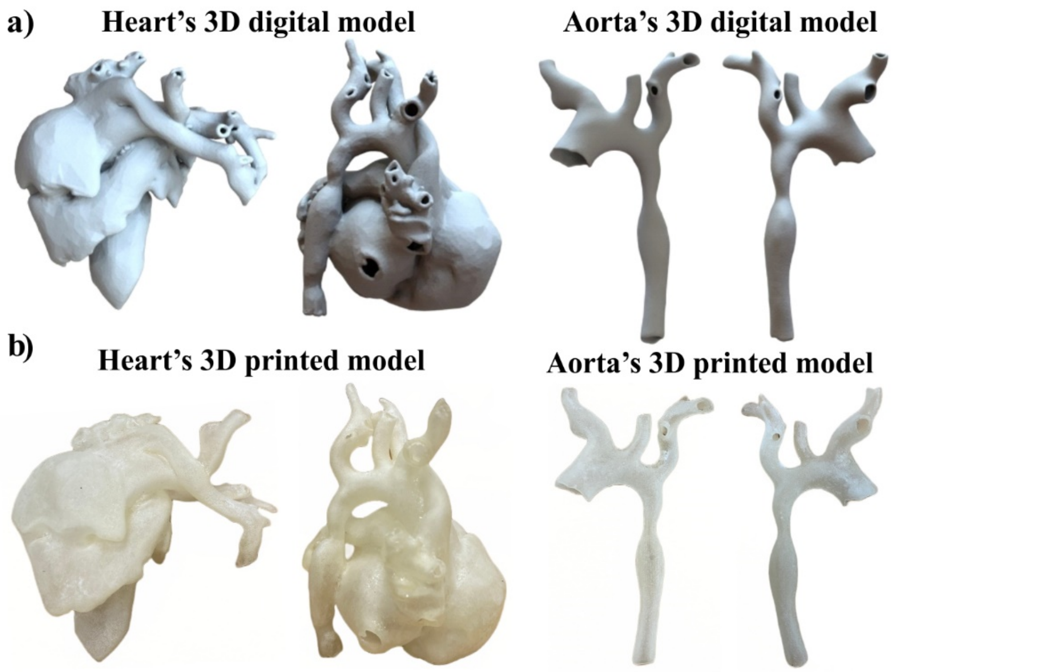

Figure 9. (**a**) Digital models and (**b**) 3D-printed models for the investigated heart and its aorta.

The 3D-printed heart-like and aorta-like structures possessed a matte amber-like color which was enhanced with the utilization of white matte powder in order to facilitate the structural light 3D scanning process. Concerning the post-processing of the 3D scanning process, registration, outlier removal, alignment, as well as fusion methods were applied in order to align these scans and extract the corresponding 3D digital models. The scanned models of the investigated heart consisted of polygon meshes with 403,102 polygons for the heart-like structure and 41,199 polygons for the aorta-like structure. In the next step, the examination of the dimensional accuracy as well as the dimensional deviation between the 3D-printed models and the 3D reconstructed models was conducted.

This was accomplished via generating SDMs of the reconstructed 3D models and the scanned models, as presented in Figure 10. The dimensional evaluation showed that both examined models were slightly smaller compared to the 3D reconstructed digital models, due to the shrinkage effect that occurred during the photo-polymerization processes. In detail, the majority of the absolute deviations were under 0.35 mm for the heart-like structure and below the value of 0.7 mm concerning the aorta-like component. Moreover, the MAE and RMSE metrics were calculated for each case, indicating the sufficient dimensional accuracy of the 3D-printed models compared to the digital ones, as it is documented in the next figure. It should be noted that the aorta-like model exhibited lower dimensional accuracy compared to the heart-like model, due to the size effect of the 3D scanning error, which increases as the size of the object becomes smaller.

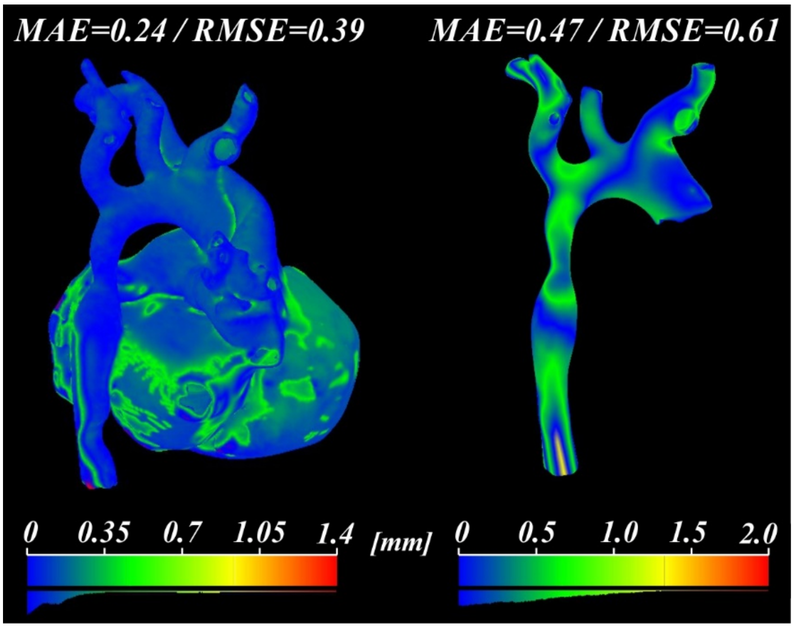

Figure 10. Surface distance maps of the manufactured human heart and aorta coupled with their dimensional accuracy metrics.

4. Conclusions

In the present study, an approach for inspecting a human heart through applying state-of-the-art technologies was introduced. Computer vision algorithms coupled with a virtual environment and computational fluid dynamics simulations were employed to examine and diagnose CT scan data that are related to various heart diseases. More specifically, an automatic 3D registration method was utilized to model DICOM data, and a segmentation methodology was used to cluster the main parts of a human heart. The main advantage of clustering the human heart is the ability to improve the diagnosis, identification, and classification of cardiac diseases. In this context, an aorta of the examined clinical case was extracted using the segmented 3D model of the investigated heart. Furthermore, the inspection of the heart was enhanced via a VR application, as well as AM technologies that were implemented to create a detailed physical model of the aortic coarctation case with sufficient dimensional accuracy, obtaining acceptable values for the MAE and RMSE metrics. To conclude, the present study introduced a promising system that is capable of constructing a 3D-printed library of personalized clinical cases using appropriate materials in order to improve preoperative assessment and train new doctors. Finally, the development of a 3D VR environment coupled with a 3D digital library of real clinical models could lead to gaining surgical experience and developing pre-operative strategies without any risk.

Author Contributions: Conceptualization, P.C. and N.K.; methodology, P.C.; software, P.C., N.K. and M.Z.; validation, P.C. and N.K.; formal analysis, P.C. and I.K.; investigation, P.C. and I.K.; resources, I.K. and K.V.; data curation, P.C.; writing—original draft preparation, P.C., N.K. and M.Z.; writing—review and editing, I.K. and D.T. (Dimitrios Tzetzis); visualization, P.C., N.K., M.Z. and K.P.; supervision, D.T. (Dimitrios Tzovaras); project administration, K.V. and D.T. (Dimitrios Tzovaras). All authors have read and agreed to the published version of the manuscript.

Funding: This research received no external funding.

Institutional Review Board Statement: Not applicable.

Informed Consent Statement: Not applicable.

Data Availability Statement: Not applicable.

Acknowledgments: This research has been co-financed by the European Union and Greek national funds through the Operational Program Competitiveness, Entrepreneurship and Innovation, under the call RESEARCH—CREATE—INNOVATE (project name 3D4KARDIA, project code: T2EDK—04012).

Conflicts of Interest: The authors declare no conflict of interest.

References

1. Kuyt, K.; Park, S.H.; Chang, T.P.; MacKinnon, R. The use of virtual reality and augmented reality to enhance cardio-pulmonary resuscitation: A scoping review. *Adv. Simul.* **2021**, *6*, 11. [CrossRef] [PubMed]
2. Pavlin-Premrl, D.; Boopathy, S.R.; Nemes, A.; Mohammadzadeh, M.; Monajemi, S.; Ko, B.S.; Campbell, C.V. Computational Fluid Dynamics in Intracranial Atherosclerosis—Lessons from Cardiology: A Review of CFD in Intracranial Atherosclerosis. *J. Stroke Cerebrovasc. Dis.* **2021**, *30*, 106009. [CrossRef] [PubMed]
3. Lopez-Jimenez, F.; Attia, Z.; Arruda-Olson, A.M.; Carter, R.; Chareonthaitawee, P.; Jouni, H.; Kapa, S.; Lerman, A.; Luong, C.; Medina-Inojosa, J.R.; et al. Artificial Intelligence in Cardiology: Present and Future. *Mayo Clin. Proc.* **2020**, *95*, 1015–1039. [CrossRef] [PubMed]
4. Brantnell, A.; Sandgren, S.; Wolff, A.; Temiz, S. Barriers and facilitators to the implementation of additive manufacturing in cardiology: A qualitative study. *Ann. 3D Print. Med.* **2022**, *7*, 100067. [CrossRef]
5. Ong, C.S.; Krishnan, A.; Huang, C.Y.; Spevak, P.; Vricella, L.; Hibino, N.; Garcia, M.A.; Gaur, L. Role of virtual reality in congenital heart disease. *Congenit. Heart Dis.* **2018**, *13*, 357–361. [CrossRef]
6. Javaid, M.; Haleem, A. Virtual reality applications toward medical field. *Clin. Epidemiol. Glob. Health* **2020**, *8*, 600–605. [CrossRef]
7. Tröbs, M.; Achenbach, S.; Röther, J.; Redel, T.; Scheuering, M.; Winneberger, D.; Klingenback, K.; Itu, L.; Passerini, T.; Kamen, A.; et al. Comparison of Fractional Flow Reserve Based on Computational Fluid Dynamics Modeling Using Coronary Angiographic Vessel Morphology Versus Invasively Measured Fractional Flow Reserve. *Am. J. Cardiol.* **2016**, *117*, 29–35. [CrossRef]
8. Celestin, C.; Guillot, M.; Ross-Ascuitto, N.; Ascuitto, R. Computational Fluid Dynamics Characterization of Blood Flow in Central Aorta to Pulmonary Artery Connections: Importance of Shunt Angulation as a Determinant of Shear Stress-Induced Thrombosis. *Pediatr. Cardiol.* **2015**, *36*, 600–615. [CrossRef]
9. Haleem, A.; Javaid, M. 3D printed medical parts with different materials using additive manufacturing. *Clin. Epidemiol. Glob. Health* **2020**, *8*, 215–223. [CrossRef]
10. Abdulmaged, A.I.; Soon, C.F.; Talip, B.A.; Zamhuri, S.A.A.; Mostafa, S.A.; Zhou, W. Characterization of Alginate–Gelatin–Cholesteryl Ester Liquid Crystals Bioinks for Extrusion Bioprinting of Tissue Engineering Scaffolds. *Polymers* **2022**, *14*, 1021. [CrossRef]
11. Kladovasilakis, N.; Charalampous, P.; Kostavelis, I.; Petsios, K.; Sarris, G.; Tzetzis, D.; Tzovaras, D. Development of heart-like structure employing additive manufacturing technologies. *Int. J. Mod. Manuf. Technol.* **2023**, *XV*. *in process*.
12. Yi, H.-G.; Lee, H.; Cho, D.-W. 3D Printing of Organs-On-Chips. *Bioengineering* **2017**, *4*, 10. [CrossRef] [PubMed]
13. Nadagouda, M.N.; Rastogi, V.; Ginn, M. A review on 3D printing techniques for medical applications. *Curr. Opin. Chem. Eng.* **2020**, *28*, 152–157. [CrossRef]
14. Osti, F.; Santi, G.M.; Neri, M.; Liverani, A.; Frizziero, L.; Stilli, S.; Maredi, E.; Zarantonello, P.; Gallone, G.; Stallone, S.; et al. CT Conversion Workflow for Intraoperative Usage of Bony Models: From DICOM Data to 3D Printed Models. *Appl. Sci.* **2019**, *9*, 708. [CrossRef]

15. Nascimento, M.C.V.; de Carvalho, A. Spectral methods for graph clustering—A survey. *Eur. J. Oper. Res.* **2011**, *211*, 221–231. [CrossRef]
16. Na, S.; Xumin, L.; Yong, G. Research on k-means Clustering Algorithm: An Improved k-means Clustering Algorithm. In Proceedings of the Third International Symposium on Intelligent Information Technology and Security Informatics, Ji'an, China, 2–4 April 2010; pp. 63–67. [CrossRef]
17. Razi, T.; Niknami, M.; Ghazani, F.A. Relationship between Hounsfield Unit in CT Scan and Gray Scale in CBCT. *J. Dent. Res. Dent. Clin. Dent. Prospect.* **2014**, *8*, 107–110. [CrossRef]
18. Nguyen, V.S.; Tran, M.H.; Quang Vu, H.M. A Research on 3D Model Construction from 2D DICOM. In Proceedings of the International Conference on Advanced Computing and Applications (ACOMP) Vietnam, Can Tho City, Vietnam, 23–25 November 2016; pp. 158–163. [CrossRef]
19. Kladovasilakis, N.; Charalampous, P.; Boumpakis, A.; Kontodina, T.; Tsongas, K.; Tzetzis, D.; Kostavelis, I.; Givissis, P.; Tzovaras, D. Development of biodegradable customized tibial scaffold with advanced architected materials utilizing additive manufacturing. *J. Mech. Behav. Biomed. Mater.* **2023**, *141*, 105796. [CrossRef]
20. Zhou, Q.Y.; Park, J.; Koltun, V. Open3D: A Modern Library for 3D Data Processing. 2018. Available online: http://www.open3d.org/ (accessed on 20 June 2023).
21. Charalampous, P.; Kostavelis, I.; Kopsacheilis, C.; Tzovaras, D. Vision-based real-time monitoring of extrusion additive manufacturing processes for automatic manufacturing error detection. *Int. J. Adv. Manuf. Technol.* **2021**, *115*, 3859–3872. [CrossRef]
22. Chen, C.; Qin, C.; Qiu, H.; Tarroni, G.; Duan, J.; Bai, W.; Rueckert, D. Deep Learning for Cardiac Image Segmentation: A Review. *Front. Cardiovasc. Med.* **2020**, *7*, 25. [CrossRef]
23. Von Luxburg, U. A tutorial on spectral clustering. *Stat. Comput.* **2007**, *17*, 395–416. [CrossRef]
24. Zelnik-Manor, L.; Perona, P. Self-tuning spectral clustering. *Adv. Neural Inf. Process. Syst.* **2004**, *17*, 1601–1608.
25. Ng, A.Y.; Jordan, M.I.; Weiss, Y. On spectral clustering: Analysis and an algorithm. *Adv. Neural Inf. Process. Syst.* **2002**, *14*, 849–856.
26. Doshi, A.R.; Chikkabyrappa, S. Coarctation of Aorta in Children. *Cureus* **2018**, *10*, e3690. [CrossRef] [PubMed]
27. Liang, C.D.; Su, W.J.; Chung, H.T.; Hwang, M.S.; Huang, C.F.; Lin, Y.J.; Chien, S.J.; Lin, I.C.; Ko, S.F. Balloon Angioplasty for Native Coarctation of the Aorta in Neonates and Infants with Congestive Heart Failure. *Pediatr. Neonatol.* **2009**, *50*, 152–157. [CrossRef]
28. Holmboe, E.S.; Durning, S.J. Assessing clinical reasoning: Moving from in vitro to in vivo. *Diagnosis* **2014**, *1*, 111–117. [CrossRef]
29. Schwarz, E.L.; Pegolotti, L.; Pfaller, M.R.; Marsden, A.L. Beyond CFD: Emerging methodologies for predictive simulation in cardiovascular health and disease. *Biophys. Rev.* **2023**, *4*, 011301. [CrossRef]
30. Marcinno, F.; Zingaro, A.; Fumagalli, I.; Dede, L.; Vergara, C. A Computational Study of Blood Flow Dynamics in the Pulmonary Arteries. *Vietnam. J. Math.* **2023**, *51*, 127–149. [CrossRef]
31. Mao, L.; Liu, J.; Hong, H.; Sun, Q.; Huang, J.; Liu, J.; Zhu, Z.; Wang, Q. Hemodynamic analysis of surgical correction for patient-specific aortic coarctation with aortic arch hypoplasia by end-to-side anastomosis. In Proceedings of the 7th International Conference on Biomedical Engineering and Informatics, Dalian, China, 14–16 October 2014; pp. 446–450. [CrossRef]
32. Castillo, M.; Marino, T. The Core Curriculum: Ultrasound. *Acad. Radiol.* **2002**, *9*, 729–730. [CrossRef]
33. Owashi, K.P.; Hubert, A.; Galli, E.; Donal, E.; Hernández, A.I.; Rolle, V. Model-based estimation of left ventricular pressure and myocardial work in aortic stenosis. *PLoS ONE* **2020**, *15*, e0229609. [CrossRef]
34. ANSYS FLUENT 12.0 Theory Guide, Standard k-ε Model. Available online: https://www.afs.enea.it/project/neptunius/docs/fluent/html/th/node58.htm (accessed on 5 September 2023).
35. Aldandarawy, A. Unity3D Cross Section Shader. 2019. Available online: https://github.com/Dandarawy/Unity3DCrossSectionShader (accessed on 20 June 2023).
36. Unity Asset Store. VRKeys. 2019. Available online: https://assetstore.unity.com/packages/tools/input-management/vrkeys-99222 (accessed on 20 June 2023).
37. Kladovasilakis, N.; Charalampous, P.; Tsongas, K.; Kostavelis, I.; Tzetzis, D.; Tzovaras, D. Experimental and Computational Investigation of Lattice Sandwich Structures Constructed by Additive Manufacturing Technologies. *J. Manuf. Mater. Process* **2021**, *5*, 95. [CrossRef]
38. Chamling, B.; Bietenbeck, M.; Drakos, S.; Korthals, D.; Vehof, V.; Stalling, P.; Meier, C.; Yilmaz, A. A compartment-based myocardial density approach helps to solve the native T1 vs. ECV paradox in cardiac amyloidosis. *Sci. Rep.* **2022**, *12*, 21755. [CrossRef] [PubMed]
39. Tanous, D.; Lee, B.N.; Horlick, E.M. Coarctation of the aorta: Evaluation and management. *Curr. Opin. Cardiol.* **2009**, *24*, 509–515. [CrossRef] [PubMed]

Disclaimer/Publisher's Note: The statements, opinions and data contained in all publications are solely those of the individual author(s) and contributor(s) and not of MDPI and/or the editor(s). MDPI and/or the editor(s) disclaim responsibility for any injury to people or property resulting from any ideas, methods, instructions or products referred to in the content.